Reduced Orthodontic Tooth Movement in *Enpp1* Mutant Mice with Hypercementosis

M. Wolf, M. Ao, M.B. Chavez, T.N. Kolli, V. Thumbigere-Math, K. Becker, E.Y. Chu, A. Jäger, M.J. Somerman, and B.L. Foster

APPENDIX

MATERIALS AND METHODS

Micro-computed Tomography (micro-CT) Analysis

Samples were scanned in a μCT 50 (Scanco Medical, Bassersdorf, Switzerland) at 70 kVp, 76 μA, and 0.5 Al filter. Mandibles from *Enpp1* mutant and WT mice at 60 dpn undergoing no orthodontic treatment were scanned at 6 μm voxel dimension with 900 ms integration time. Crania with maxillae from mice undergoing orthodontic treatment were scanned at 10-17 μm voxel dimension with 300 ms integration time. DICOM files were created and exported from scan data and calibrated to five known densities of hydroxyapatite (mg/cm^3 HA) for mineral density analysis. Reconstructed images were loaded and analyzed in Amira software (version 6.1.2; FEI, Berlin, Germany) or AnalyzePro (version 1.0; AnalyzeDirect, Overland Park, KS, USA).

Mandibles were reoriented to a standard position in 3D space using first molar anatomical landmarks (Foster et al. 2017). In mid-molar sagittal section, a line through mesial and distal cemento-enamel junctions (CEJ) was made parallel to the transverse plane. In mid-root (halfway from CEJ to apex) transverse section, mesial and distal roots were made parallel to the sagittal plane. In mid-root coronal section, the mesial root canal was made parallel to the z-axis. The region of interest (ROI) for analysis (first molar and surrounding PDL and bone) was

then defined by cropping the mandible 480 μm mesial and distal from the most mesial and distal aspects of the first molar cusps (Appendix Figure 1A, B). This ROI was defined to include the mesial rise of the alveolar bone in the diastema and the interproximal bone between the first and second molars. No post-processing beam hardening corrections were performed on mandibles for analysis. Bone and teeth were automatically segmented and separated with a density above 650 mg/cm^3 HA. Further subdivision of mandibular bone divided bone into two regions, alveolar bone and basal bone. Alveolar bone was defined as being adjacent to the molar roots while basal bone was defined as bone apical of the most apical aspect of the distal root. PDL was semi-automatically traced from CEJ apically around the entire molar root. PDL volume was determined around the entire first maxillary molar tooth by excluding tooth and bone in the ROI. A more defined ROI was selected for more detailed measurements of PDL width and area: 50 transverse slices (300 μm) of the mesial root and PDL were cropped from the midpoint of the root as measured from CEJ to apex. This ROI was used to determine PDL width (average tooth-bone distance), cementum-PDL interface surface area (surface area at the interface of tooth root and PDL within the defined ROI), and bone-PDL interface surface area (surface area at the interface of alveolar bone and PDL within the defined ROI). These measurements were found using cortical algorithms used more extensively in cortical bone analysis (Bouxsein et al. 2010).

Representative images of orthodontically treated crania shown in Figures 1 and 3 were processed by median filter kernel size 7 to remove beam hardening artifacts from scanning. Samples processed this way were not used for quantitative analyses. Orthodontically treated

crania with maxillae were reoriented as cropped hemi-crania by rotating the transverse plane of the left orthodontic tooth movement (OTM) side so that the distal root in the sagittal plane had the smallest compression zone on the mesial aspect and largest tension zone on the distal aspect. The angle of reorientation was mirrored on the right contralateral control (CC) side. Mesial tooth movement was measured using a modification of a method described previously (Gonzales et al. 2009). In brief, the linear distance between treated first and untreated second molars was quantified by a three-point measurements surrounding the contact point. Effect of tooth movement on alveolar bone height was evaluated mesial to treated molars. Vertical distances between alveolar bone crest (ABC) and CEJ were measured and changes were defined by comparison of treated and untreated sides (Gonzales et al. 2009).

Measurements were made of periodontal tissues on mesial and distal aspects (compression and tension sides on OTM side) of the distal root of first molars on OTM and CC sides. PDL was traced from ABC to root apex for the 3 most midsagittal slices of the mesial and distal aspects of the distal root. PDL width was measured linearly down the middle of the PDL from ABC to apex to determine average width of the PDL (Appendix Figure 1C). To determine bone mineral density (BMD), 20 transverse slices of alveolar bone were segmented at the mid length as measured from CEJ to apex of the distal root and extended 0.05 mm in both the mesial and distal directions to define the ROIs.

REFERENCES

Bouxsein ML, Boyd SK, Christiansen BA, Guldberg RE, Jepsen KJ, Muller R. 2010. Guidelines for assessment of bone microstructure in rodents using micro-computed tomography. J Bone Miner Res. 25(7):1468-1486.

Foster BL, Ao M, Salmon CR, Chavez MB, Kolli TN, Tran AB, Chu EY, Kantovitz KR, Yadav M, Narisawa S et al. 2017. Osteopontin regulates dentoalveolar mineralization. In review.

Gonzales C, Hotokezaka H, Arai Y, Ninomiya T, Tominaga J, Jang I, Hotokezaka Y, Tanaka M, Yoshida N. 2009. An in vivo 3d micro-ct evaluation of tooth movement after the application of different force magnitudes in rat molar. Angle Orthod. 79(4):703-714.

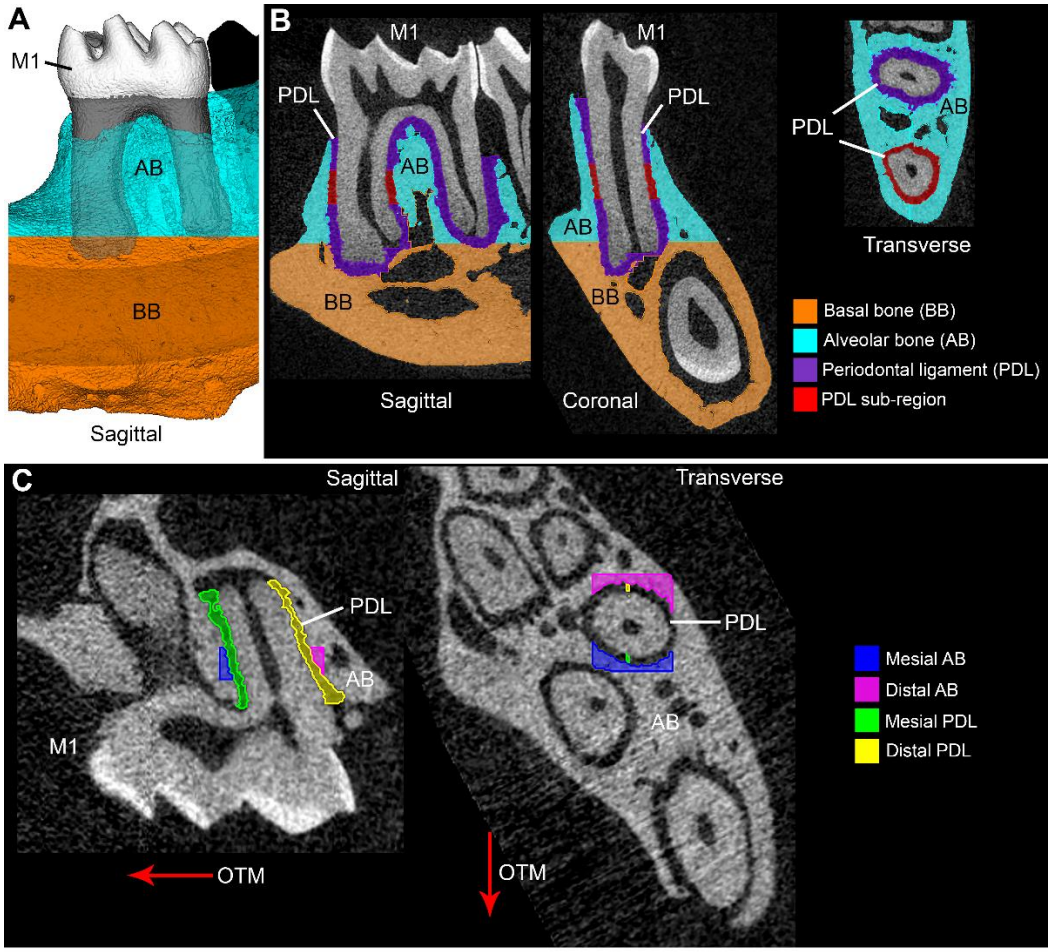

Appendix Figure 1. Microcomputed tomography analysis of dentoalveolar tissues. Panels A and B indicate regions of interest (ROI) for analysis of mouse mandibles, while panel C indicates ROI for maxillae on contralateral control (CC) side or following orthodontic tooth movement (OTM). **(A)** For 3D quantitative analysis of the first mandibular molar (M1) and surrounding tissues by microcomputed tomography (micro-CT), mandibles were reoriented to a standard position with a vertical position of the mesial root. **(B)** In mid-molar sagittal section (left panel), mid-mesial root coronal section (middle panel), and mid-root transverse section (right panel) of M1, tissue subdivisions are shown for basal bone (BB; orange), alveolar bone (AB; light blue), periodontal ligament (PDL; purple), and PDL sub-region width on the mesial root (red). **(C)** For 3D quantitative analysis of first maxillary molar (M1) by micro-CT (shown in both sagittal and transverse orientations), measurements were made of periodontal tissues on mesial and distal aspects of the distal root of first molars on OTM and CC sides. PDL was traced from alveolar bone crest to root apex for the 3 most midsagittal slices of the mesial and distal aspects of the distal root, and PDL width was measured linearly down the middle of the PDL to determine average width on mesial (green) and distal (yellow) aspects. To determine bone mineral density (BMD), 20 transverse slices of alveolar bone were segmented at the mid length as measured from cementum-enamel junction to apex of the distal root and extended 0.05 mm in both the mesial (blue) and distal (pink) directions to define the ROIs. Red arrows in C indicate mesial direction of OTM.

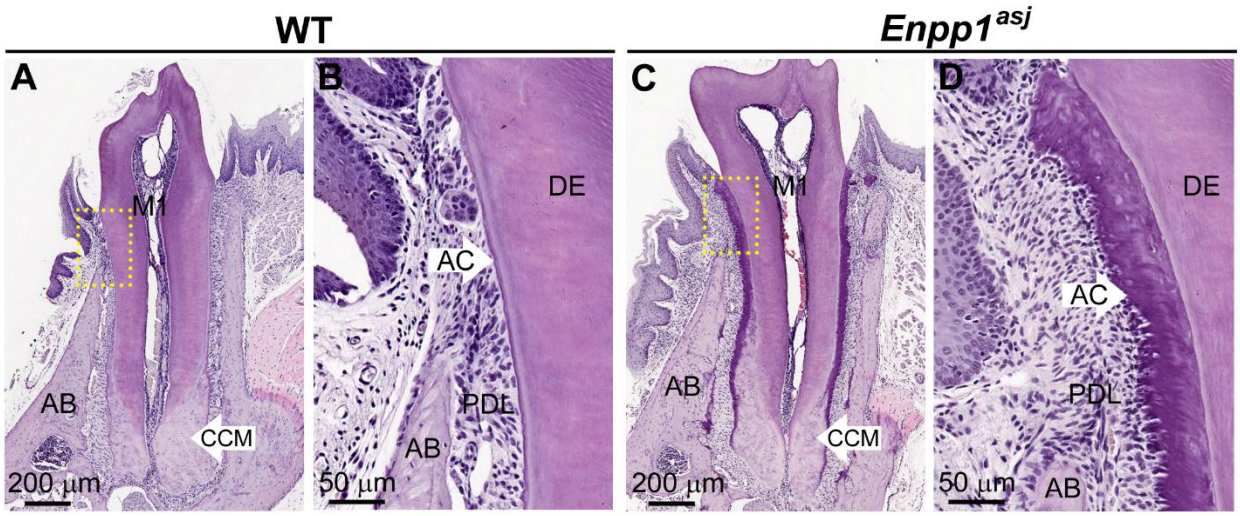

Appendix Figure 2. ***Enpp1*** **mutant mice exhibit hypercementosis.** Histology performed on mandibles from mice at 60 dpn reveals that compared to **(A, B)** WT controls, **(C, D)** *Enpp1*^{asj} mice feature dramatically increased acellular cementum (AC) on cervical root surfaces of first mandibular molars (M1). Note the inclusion of cementocyte-like cells in this thick cervical cementum in *Enpp1*^{asj} mice, whereas cementum at this location typically remains as a thin, cell-free tissue layer. Yellow dotted boxes in panels A and C indicate locations shown at high magnification in panels B and D. AB=alveolar bone; PDL=periodontal ligament; CCM=cellular cementum; DE=dentin.

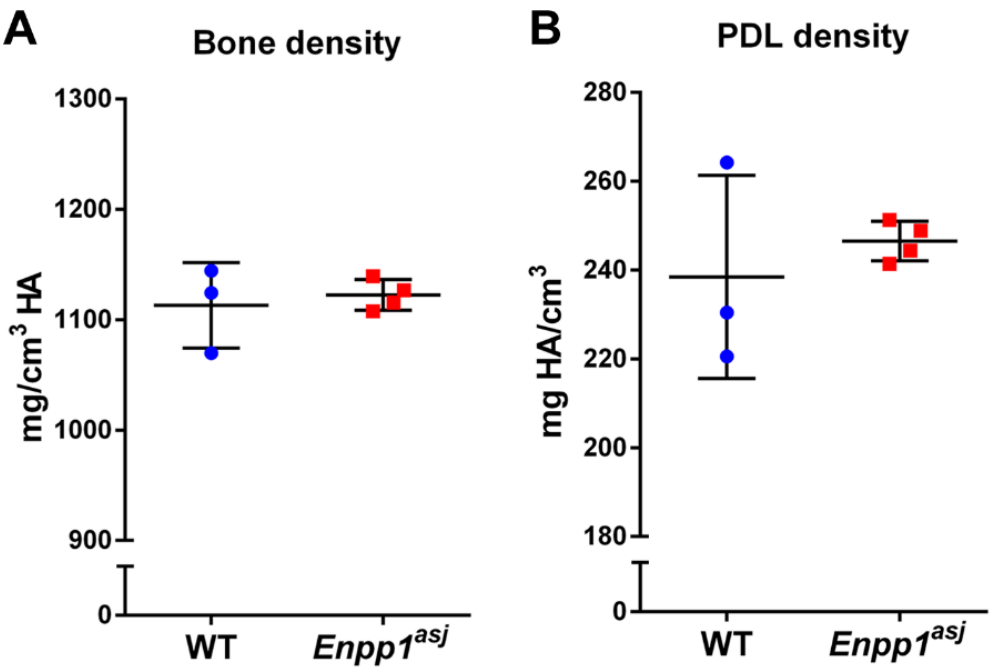

Appendix Figure 3. Micro-CT analysis of periodontal tissues. Quantitative 3D micro-CT analysis revealed no differences in **(A)** alveolar bone density or **(B)** periodontal ligament (PDL) tissue density around first molars in WT vs. *Enpp1*^{asj} mice at 60 dpn.

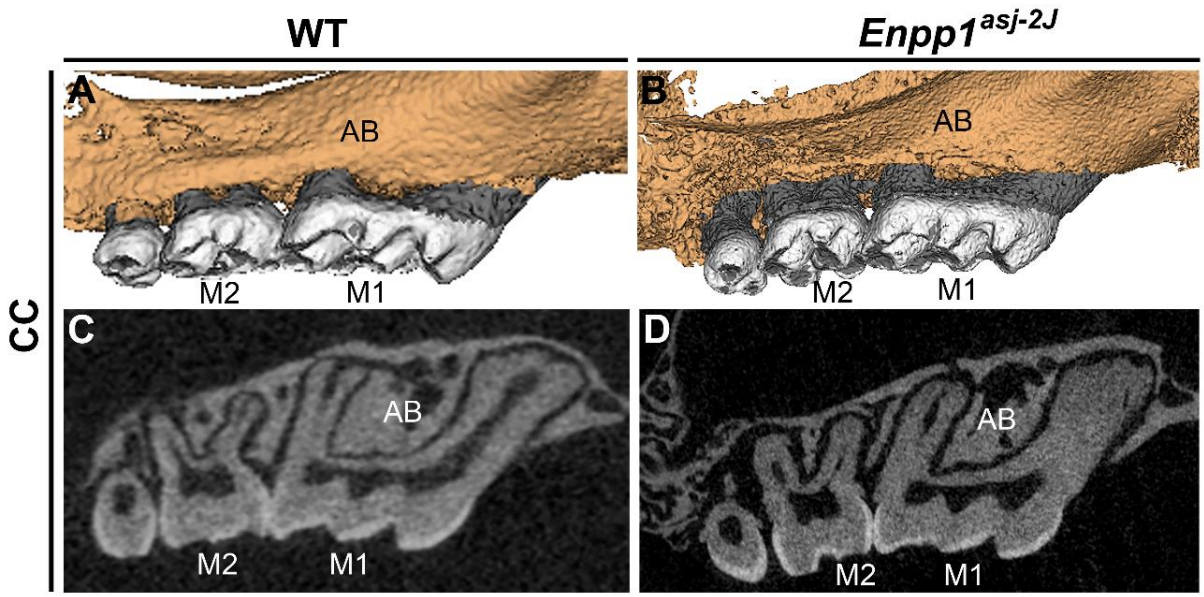

Appendix Figure 4. Tooth position on contralateral control side. (A, B) 3D and **(C, D)** 2D views of contralateral control (CC) sides of WT and *Enpp1*$^{asj\text{-}2J}$ mouse maxillae for comparison to orthodontic toot movement (OTM) sides in Figure 3. Note proximity of crowns of first and second molars (M1 and M2) on CC sides.

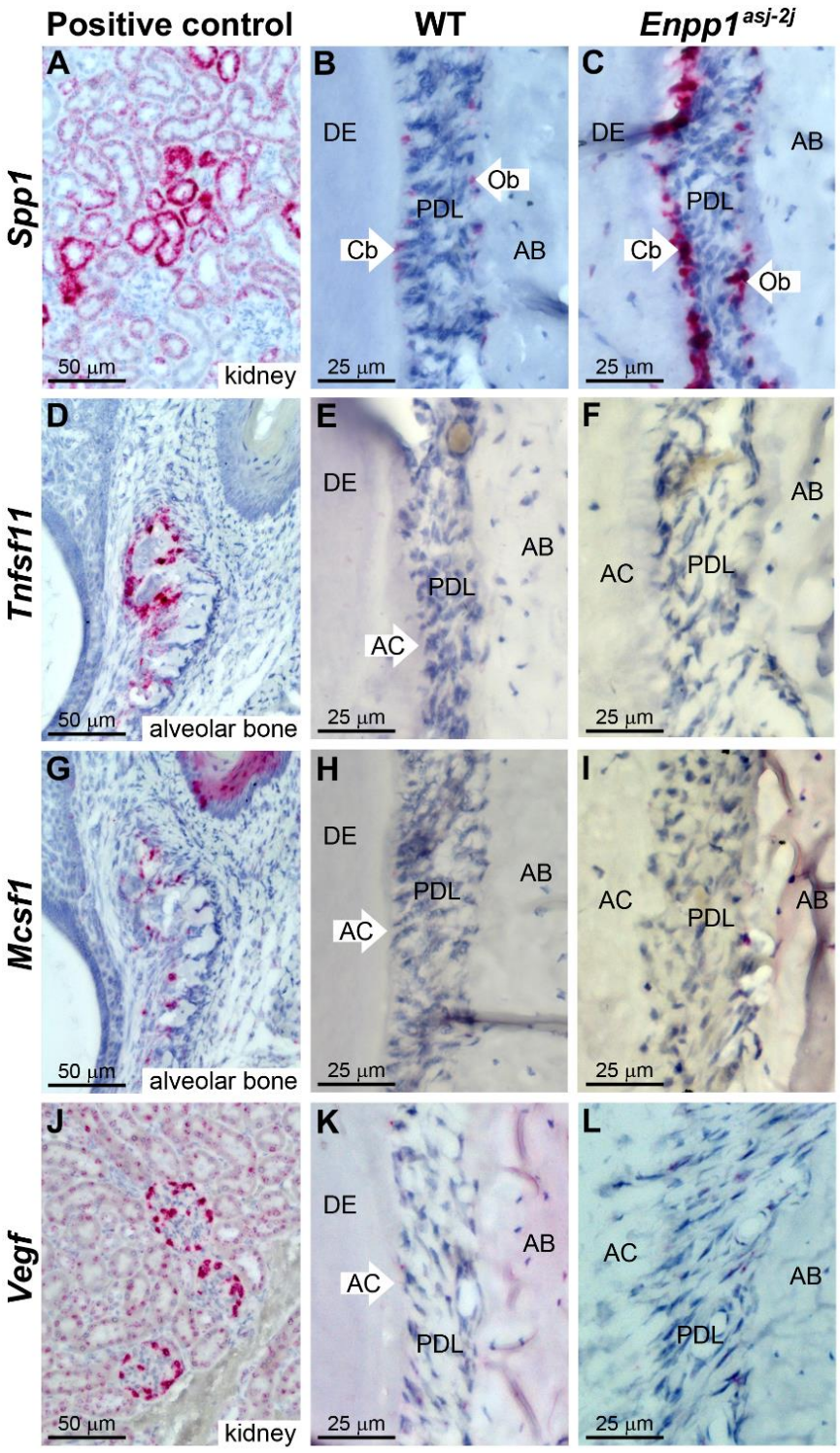

Appendix Figure 5. Altered Spp1 mRNA expression in Enpp1 mutant mouse cementoblasts. *In situ* hybridization (ISH) was performed using positive control tissues for **(A)** *Spp1* (kidney), **(D)** *Tnfsf11* (resorbing alveolar bone around erupting mouse molar at 14 dpn), **(G)** *Mcsf1* (resorbing alveolar bone around erupting mouse molar at 14 dpn), and **(J)** Vegf (kidney). **(B)** Untreated

WT mouse periodontal tissues at 60 dpn showed low *Spp1* expression in cementoblasts (Cb) of acellular cementum and osteoblasts (Ob) of alveolar bone (AB). **(C)** In *Enpp1*$^{asj\text{-}2J}$ mouse periodontal tissues, *Spp1* expression was dramatically in Cb, and to a lesser degree in Ob. In both WT and *Enpp1*$^{asj\text{-}2J}$ mouse periodontal tissues, no substantial mRNA expression was found for **(E, F)** *Tnfsf11*, **(H, I)** *Mcsf1*, or **(K, L)** *Vegf*. DE=dentin; PDL=periodontal ligament.